Downloaded from jnm.snmjournals.org by on March 14, 2017. For personal use only.

Assessment of Hypoxia and Perfusion in Human Brain Tumors Using PET with ^{18}F-Fluoromisonidazole and ^{15}O-H_2O

Matthias Bruehlmeier, MD[1,2]; Ulrich Roelcke, PhD, MD[3]; Pius A. Schubiger, PhD[1]; and Simon Mensah Ametamey, PhD[1]

[1]Paul Scherrer Institute, Center for Radiopharmaceutical Science, Villigen, Switzerland; [2]Department of Nuclear Medicine, Cantonal Hospital Aarau, Aarau, Switzerland; and [3]Department of Neurology, Cantonal Hospital Aarau, Aarau, Switzerland

Hypoxia predicts poor treatment response of malignant tumors. We used PET with ^{18}F-fluoromisonidazole (^{18}F-FMISO) and ^{15}O-H_2O to measure in vivo hypoxia and perfusion in patients with brain tumors. **Methods:** Eleven patients with various brain tumors were investigated. We performed dynamic ^{18}F-FMISO PET, including arterial blood sampling and the determination of ^{18}F-FMISO stability in plasma with high-performance liquid chromatography (HPLC). The ^{18}F-FMISO kinetics in normal brain and tumor were assessed quantitatively using standard 2- and 3-compartment models. Tumor perfusion (^{15}O-H_2O) was measured immediately before ^{18}F-FMISO PET in 10 of the 11 patients. **Results:** PET images acquired 150–170 min after injection revealed increased ^{18}F-FMISO tumor uptake in all glioblastomas. This increased uptake was reflected by ^{18}F-FMISO distribution volumes >1, compared with ^{18}F-FMISO distribution volumes <1 in normal brain. The ^{18}F-FMISO uptake rate K_1 was also higher in all glioblastomas than in normal brain. In meningioma, which lacks the blood–brain barrier (BBB), a higher K_1 was observed than in glioblastoma, whereas the ^{18}F-FMISO distribution volume in meningioma was <1. Pixel-by-pixel image analysis generally showed a positive correlation between ^{18}F-FMISO tumor uptake at 0–5 min after injection and perfusion (^{15}O-H_2O) with *r* values between 0.42 and 0.86, whereas late ^{18}F-FMISO images (150–170 min after injection) were (with a single exception) independent of perfusion. Spatial comparison of ^{18}F-FMISO with ^{15}O-H_2O PET images in glioblastomas showed hypoxia both in hypo- and hyperperfused tumor areas. HPLC analysis showed that most of the ^{18}F-FMISO in plasma was still intact 90 min after injection, accounting for 92%–96% of plasma radioactivity. **Conclusion:** Our data suggest that late ^{18}F-FMISO PET images provide a spatial description of hypoxia in brain tumors that is independent of BBB disruption and tumor perfusion. The distribution volume is an appropriate measure to quantify ^{18}F-FMISO uptake. The perfusion–hypoxia patterns described in glioblastoma suggest that hypoxia in these tumors may develop irrespective of the magnitude of perfusion.

Key Words: brain tumor; hypoxia; ^{18}F-fluoromisonidazole; PET

J Nucl Med 2004; 45:1851–1859

Hypoxia is defined as a reduction of intracellular oxygen pressure (pO_2) as a result of decreased supply of and increased demand for oxygen. pO_2 levels in normal tissue generally exceed 40 mm Hg, and severe hypoxia may be present in malignant tumors (*1*). Levels of $pO_2 < 3$ mm Hg are associated with impaired response to radiotherapy (*2*). Two different forms of tumor hypoxia are recognized. Diffusion-limited chronic hypoxia may develop as a result of increased intercapillary distances, and acute hypoxia can result from occlusion of large tumor vessels (*3*). Either form of hypoxia has several implications for the further evolution of tumors (e.g., by induction of signaling cascades that promote angiogenesis, growth, and cell migration) (*4*). Tumor hypoxia may also lead to necrosis, which is mandatory to establish the diagnosis in glioblastoma multiforme (*5*). In brain tumors, the presence of hypoxia has been inferred from pathologic examination of tumor tissue, from animal models, and from MRI of malignant gliomas that indicate necrosis (*5–7*).

In vivo measurement of hypoxia in individual patients is of clinical interest. It could provide insight into the natural course and pathophysiology of tumors, possibly assisting in the planning of radio- and chemotherapy and in the evaluation of treatment response. Noninvasive methods to measure tumor hypoxia with PET or SPECT are available with ^{18}F-fluoromisonidazole (^{18}F-FMISO) or other radioligands (*8–13*).

^{18}F-FMISO is a nitroimidazole derivative, which to our knowledge was the first PET agent used for hypoxia detection in a larger cohort of patients with tumors outside the central nervous system (*14*). ^{18}F-FMISO PET can image tumor hypoxia by increased ^{18}F-FMISO tumor uptake, because ^{18}F-FMISO metabolites are trapped exclusively in hypoxic cells (*15*). In tumor hypoxia, the ^{18}F-FMISO tumor concentration measured by PET typically exceeds ^{18}F-

Received Jan. 8, 2004; revision accepted May 27, 2004.

For correspondence or reprints contact: Matthias Bruehlmeier, MD, Department of Nuclear Medicine, Cantonal Hospital Aarau, CH-5001 Aarau, Switzerland.

E-mail: matthias.bruehlmeier@ksa.ch

Downloaded from jnm.snmjournals.org by on March 14, 2017. For personal use only.

FMISO plasma concentration as measured during PET. Because ^{18}F-FMISO is relatively lipophilic, with an octanol water coefficient (log P) of 0.4, it diffuses through cell membranes and shows a passive distribution in normal tissue. Therefore, with the exception of the liver, the intestines, the kidney, and the bladder, the ^{18}F-FMISO concentration in normal, nonhypoxic tissue is always lower than in plasma.

The results of ^{18}F-FMISO PET studies of 3 patients with glioblastoma multiforme have been reported by Valk et al. (*16*). In the pilot study presented here, we measured hypoxia in different human brain tumors using PET and ^{18}F-FMISO. In addition, because gliomas show a large range of tumor blood flow, we investigated the influence of tumor perfusion on ^{18}F-FMISO kinetics and on the presence of hypoxia by means of ^{15}O-H_2O PET (*17*). ^{18}F-FMISO PET scans were performed quantitatively to determine the ^{18}F-FMISO distribution volume and transport rate constants in normal brain and in brain tumors.

MATERIALS AND METHODS

Patients

Eleven patients were selected at the Cantonal Hospital (Aarau, Switzerland). T2-weighted and gadolinium-enhanced T1-weighted MR images were available for all patients. All patients, with a single exception, exhibited either residual or recurrent tumor after surgery, with signs of tumor progression on MR images or appearance of a new lesion. Of the 7 patients with glioblastoma, 6 completed radiotherapy before the PET study, and 5 patients had received 4–6 cycles of temozolomide chemotherapy. At the time of the PET study, 5 patients were receiving oral dexamethasone (mean, 4 mg/d). The meningioma patient was included to address the ^{18}F-FMISO kinetics in a brain tumor that lacks a blood–brain barrier (BBB). All patients gave written consent for participation in the study. The study protocol was approved by the Ethical Committee at the Cantonal Hospital Aarau.

^{18}F-FMISO and ^{15}O-H_2O PET Scanning

The radiosynthesis of ^{18}F-FMISO was performed according to the 2-step procedure reported by Lim et al. (*18*). The total synthesis time was approximately 120 min, and radiochemical purity was >99%. Specific radioactivities were also always >30 GBq/μmol.

All PET studies were performed on a whole-body scanner (Advance; General Electric Medical Systems), where 35 reconstructed planes cover an axial field of view of 14.6 cm and the reconstructed in-plane resolution is 7 mm. Catheters were placed into a radial artery under local anesthesia and in a vein of the contralateral arm. For PET, the patient's head was fixed in a special holder. First, a 10-min transmission scan with 2 rotating ^{68}Ge line sources was performed for attenuation correction. Then, 500–700 MBq ^{15}O-H_2O were injected intravenously as a bolus, and a static 60-s PET scan was started when the radioactivity in the head exceeded 100,000 counts per second as measured by the scanner (a ^{15}O-H_2O scan could not be performed in 1 patient because of a malfunction of the cyclotron during the PET imaging). After waiting 10 min to allow sufficient decay of ^{15}O, an average of 291 MBq ^{18}F-FMISO (range, 123–421 MBq) were infused intravenously during 3 min using a constant volume infusion pump. ^{18}F-FMISO infusion was preferred to a bolus injection, because it permitted manual drawing of blood samples for precise measurement of the arterial input curve, including the radioactivity peak after injection. A device to record the arterial input curve online in real time was not available. For this reason, arterial blood measurements were not performed during the ^{15}O-H_2O PET scan. Simultaneous with the start of ^{18}F-FMISO infusion, a dynamic PET scan was acquired, consisting of 31 frames with a total scan duration of 90 min. The PET time frames were 9 × 20, 4 × 30, 2 × 60, 4 × 120, 9 × 300, and 3 × 600 s. During the PET scan, 26 arterial blood samples of 4 mL each were drawn, and the radioactivity of both whole blood and plasma was measured using a well counter. The blood samples were drawn at 0.5, 1, 1.5, 2, 2.5, 3, 3.5, 4, 4.5, 5, 5.5, 6, 7, 8, 9, 10, 12.5, 15, 17.5, 20, 25, 30, 40, 50, 60, and 75 min after injection. After resting approximately 45 min, the patients were repositioned on the PET scanner. A second 10-min transmission scan was acquired, followed by a static 20-min emission scan exactly 150–170 min after injection of ^{18}F-FMISO.

Generally, image processing used a minimum of filtering. In the case of dynamic ^{18}F-FMISO scans, filtering was not necessary, because adding the last 3 PET time frames resulted in sufficient image quality to draw the regions of interest (ROIs). The ^{15}O-H_2O images required a 3-dimensional gaussian filter with a full width at half maximum (FWHM) of 8 mm and for the static ^{18}F-FMISO images a filter of FWHM 5 mm. Blood measurements were decay corrected to the time of ^{18}F-FMISO injection. We performed a standard cross-calibration between PET images and blood radioactivity by measuring the radioactivity of a known amount of ^{18}F-FMISO in a water phantom with both the PET scanner and a γ-well counter.

Image Coregistration and ROIs

For coregistration of ^{15}O-H_2O images with the first ^{18}F-FMISO scan, no spatial corrections were necessary because of the fixed head position during both scans. The 31 frames of the first ^{18}F-FMISO PET scan were examined for motion artifacts. A spatial correction was necessary to coregister the second ^{18}F-FMISO scan with the first. For that purpose, the last 3 frames of the first scan (60–90 min after injection) were added, allowing delineation of the brain contours and those tumors that accumulated ^{18}F-FMISO. These landmarks were used for a manual coregistration of both ^{18}F-FMISO scans using the software PMOD (PMOD Technologies Ltd.) (*19*).

For an analysis of ^{18}F-FMISO kinetics in normal brain, we placed ROIs of identical size in the contralateral frontal cortex, frontal white matter, and cerebellum. ROI sizes were 7.28 (312 voxels), 4.04 (173 voxels), and 18.23 mL (781 voxels) for white matter, frontal cortex, and cerebellum, respectively. Tumor ROIs in all glioblastomas (n = 7) and in the hemangioblastoma were placed on areas with increased ^{18}F-FMISO uptake as determined by late images. These ROIs did not cover the whole tumor area but included presumably hypoxic tumor areas. In another patient with a meningioma, the tumor was delineated only in early PET images 0–30 min after injection, and these images were consequently used to define the tumor ROI. Tumor ROIs were placed on multiple transverse slices and then summed up to a 3-dimensional ROI. Sizes of these tumor ROIs were 0.86, 1.63, 2.12, 0.37, 2.12, 1.24, and 4.34 mL (37, 70, 91, 16, 91, 53, and 186 voxels, respectively) for patients 1–7, 0.86 mL (37 voxels) for patient 10, and 1.70 mL (73 voxels) for patient 11.

Downloaded from jnm.snmjournals.org by on March 14, 2017. For personal use only.

For a pixel-per-pixel correlation between ^{15}O-H_2O and ^{18}F-FMISO PET images, a different set of tumor ROIs was defined to minimize the possibility of including surrounding normal brain tissue. These ROIs were placed only on a single transverse slice showing the maximum tumor diameter, so that it covered the whole tumor area with variably increased ^{18}F-FMISO uptake.

PET Data Analysis

Decay-corrected time–activity curves were derived from the first ^{18}F-FMISO PET scan from 0 to 90 min after injection. The radioactivity of normal brain and tumor was plotted against time after injection and the time–activity curves were used for kinetic modeling to calculate the ^{18}F-FMISO transport rates and distribution volume in 2- and 3-compartment models (Appendix). In addition, we applied Logan plots in normal brain and in tumor, with DV_{Logan} as a measure of the distribution volume of ^{18}F-FMISO independent of assumptions about the number of underlying tissue compartments (*20*). The second, static ^{18}F-FMISO PET scan was also evaluated by ROI analysis (i.e., ratios of tumor and cerebellum radioactivity were calculated).

^{15}O-H_2O PET images were analyzed semiquantitatively, and perfusion in tumor hypoxia was graded as: 1 = lower than white matter; 2 = equal to white matter; 3 = between white matter and cortex; 4 = equal to cortex; 5 = higher than cortex. For the purpose of comparing hypoxia with perfusion, hypoxic tumor areas were delineated on late ^{18}F-FMISO PET images, and the resulting ROIs were transferred to the coregistered ^{15}O-H_2O PET images. In addition, a pixel-per-pixel correlation between ^{15}O-H_2O and ^{18}F-FMISO images was performed. Pixel values in a tumor ROI were normalized to their own maximum, and relative ^{18}F-FMISO uptake at 0–5, 60–90, and 150–170 min after injection was plotted against relative ^{15}O-H_2O uptake.

Measurement of ^{18}F-FMISO Stability in Plasma and Urine

For measurement of ^{18}F-FMISO plasma stability, 0.6 mL of a solution containing 3% perchloric acid (60%; Merck), 1% $Na_2S_2O_5$ (Merck), and 0.1% ethylenediaminetetraacetic acid (Fluka) were added to 0.5 mL plasma for protein precipitation. The solution was centrifuged at 4,800 rpm during 5 min, and 1 mL of the supernatant was submitted to high-performance liquid chromatography (HPLC) using a Merck Hitachi L-6200A Intelligent Pump and a Bondclone 10 C18 column. We used a solution containing 80% water and 20% acetonitrile for elution; flow was set to 0.5 mL/min. The eluate was collected by a 2112 Redirac fraction collector in 100 samples during a total elution time of 30 min. The radioactivity of each sample was measured in a γ-well counter (Cobra II Auto Gamma; Camberra Packard) and was plotted against elution time. ^{18}F-FMISO metabolites in urine were measured similarly, with the exception that no protein precipitation was performed. In addition, the retention time of intact ^{18}F-FMISO was determined in several HPLC experiments using an aliquot of the ^{18}F-FMISO injection solution. Using knowledge of the normal retention time of intact ^{18}F-FMISO, radioactive metabolites in plasma and urine were visually discriminated from the ^{18}F-FMISO peak on the HPLC plots, and the amount of metabolites and intact ^{18}F-FMISO were expressed as a percentage of total radioactivity in the chromatogram.

RESULTS

Clinical data are presented in Table 1 . Examples of MR and ^{18}F-FMISO PET images are shown in Figure 1, where the glioblastoma multiforme exhibited increased ^{18}F-FMISO uptake at late scan time (150–170 min after injection). In contrast, the meningioma showed higher ^{18}F-FMISO uptake than surrounding brain only during the first 30 min after injection. Time–activity curves of the same 2 patients are depicted in Figure 2, showing that the radioactivity in the glioblastoma begins to exceed plasma radioactivity approximately 30 min after injection, whereas the radioactivity in the meningioma did not exceed plasma radioactivity at any time. In normal brain, the radioactivity of cortex and white matter slowly approached the radioactivity in plasma, a finding that is representative for all patients.

In normal brain, the kinetics of ^{18}F-FMISO generally satisfied a 2-compartment model with the distribution volume ($DV' < 1$ in all regions, indicating a passive distribution and reflecting a homogeneous ^{18}F-FMISO uptake in

TABLE 1
Summary of Clinical Data

Patient	Sex	Age (y)	Resection type	Histology	Time of PET after surgery (wk)	Radiotherapy	Chemotherapy (no. of cycles)
1	M	50	B	Glioblastoma	42	Yes	No
2	F	67	P	Glioblastoma	(PET preoperative)	No	No
3	F	42	GT	Glioblastoma	21	Yes	Temozolomide (6)
4	M	45	GT	Glioblastoma	30	Yes	Temozolomide (6)
5	M	56	GT	Glioblastoma	28	Yes	Temozolomide (5)
6	M	54	GT	Glioblastoma	54	Yes	Temozolomide (4)
7	M	64	GT	Glioblastoma	20	Yes	Temozolomide (4)
8	M	31	GT	Anaplastic astrocytoma	53	No	No
9	M	24	GT	Fibrillary astrocytoma	57	No	No
10	M	39	GT	Hemangioblastoma	122	Yes	No
11	F	67	B	Meningioma	151	No	No

B = biopsy; P = partial resections; GT = gross total resection.

Downloaded from jnm.snmjournals.org by on March 14, 2017. For personal use only.

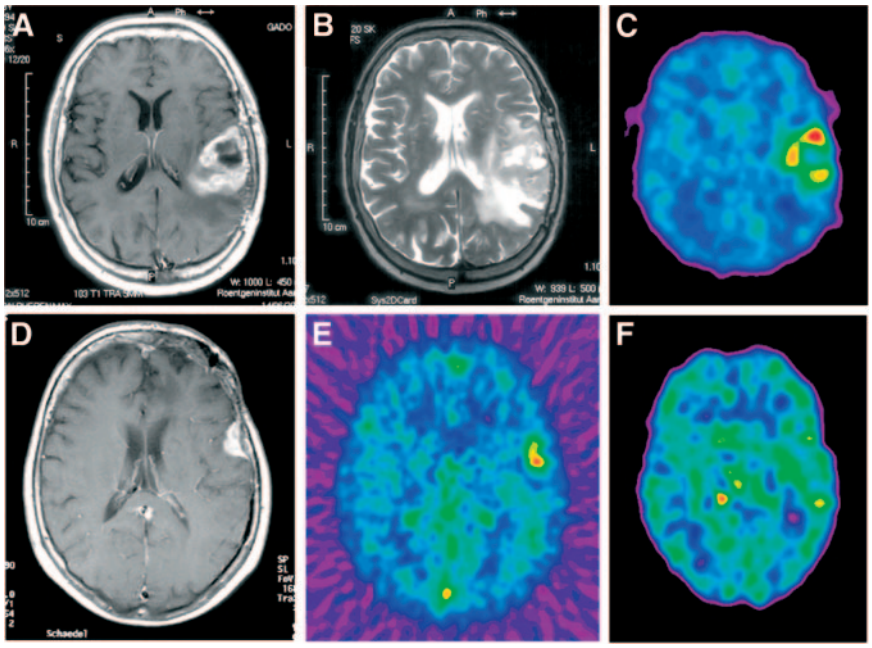


FIGURE 1. (A and B) Gadolinium contrast-enhanced T1- and T2-weighted MR images in patient with glioblastoma multiforme in left temporal lobe. (C) Late PET images show ^{18}F-FMISO tumor uptake 150–170 min after injection. (D) Gadolinium contrast-enhanced T1-weighted MR image of patient with meningioma in left temporal lobe. (E) ^{18}F-FMISO uptake in meningioma is visible in early PET image 0–5 min after injection but not in late PET images 150–170 min after injection (F). PET images are normalized to their own maximum.

the cerebrum and cerebellum at late scan time (Table 2). In tumor, increased ^{18}F-FMISO uptake was observed at late scan time in all glioblastoma multiforme and in the hemangioblastoma but not in the anaplastic astrocytoma (World Health Organization tumor classification III [WHO III]), a fibrillary astrocytoma (WHO II), or a meningioma. Tumor areas with increased uptake showed an ^{18}F-FMISO distribution volume (DV_{TOT}) > 1 in the 3-compartment model (Table 3). Determination of the ^{18}F-FMISO distribution volume using a Logan plot resulted in DV_{Logan} values that were slightly smaller than DV_{TOT} in 5 of 7 tumors. Notably, DV_{Logan} was <1 in 2 patients despite increased ^{18}F-FMISO uptake and $DV_{TOT} > 1$. Ratios of tumor and cerebellum radioactivity in the static late PET image were comparable with DV_{TOT} values (Table 3).

Visual comparison of ^{15}O-H_2O with late ^{18}F-FMISO PET images in 6 patients with glioblastoma showed a large range of tumor perfusion within areas with increased ^{18}F-FMISO uptake (i.e., increased ^{18}F-FMISO uptake was found both in hypo- and hyperperfused tumor areas (Fig. 3; Table 3). Generally, increased ^{18}F-FMISO uptake was found in the tumor margin but not in the tumor center. Tumor centers of all glioblastomas showed decreased radioactivity in both ^{15}O-H_2O and ^{18}F-FMISO PET images.

Pixel-per-pixel correlations between ^{15}O-H_2O and ^{18}F-FMISO images were performed in 5 of the glioblastoma patients (example in Fig. 4). At 0–5 min after injection, ^{18}F-FMISO uptake was positively correlated with perfusion in 4 of 5 cases. The correlation coefficients (r values) in these patients were 0.69, 0,02, 0.42, 0.74, and 0.86. This correlation was no longer evident at 60–90 min after injection in 3 of 5 patients but persisted in 2 patients. With a single exception, no correlation was found at 150–170 min after injection, when the r values were 0.02, 0.10, 0.61,

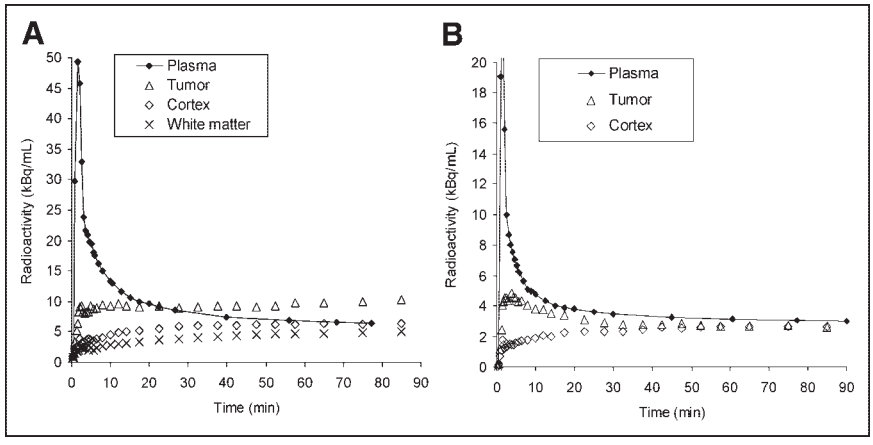


FIGURE 2. Time–activity curves of ^{18}F-FMISO PET scans in patient with glioblastoma (A) and patient with meningioma (B), corresponding to PET images shown in Figure 1. Plasma = radioactivity concentration in arterial plasma during PET.

Downloaded from jnm.snmjournals.org by on March 14, 2017. For personal use only.

TABLE 2
^{18}F-FMISO PET Results in Normal Brain

Contralateral normal tissue	2-Compartment model and Logan plot				3-Compartment model				
	K_1'	k_2'	DV′	DV_{Logan}	k_1	k_2	k_3	k_4	DV_{tot}
Cerebellum									
Mean	0.027	0.031	0.858	0.859	0.031	0.045	0.015	0.058	0.858
SD	0.005	0.006	0.059	0.061	0.003	0.001	0.006	0.014	0.066
Frontal lobe cortex									
Mean	0.023	0.029	0.813	0.833	0.026	0.049	0.027	0.037	0.867
SD	0.003	0.004	0.064	0.064	0.002	0.010	0.024	0.013	0.071
Frontal lobe white matter									
Mean	0.010	0.012	0.883	0.730	—	—	—	—	—
SD	0.002	0.004	0.151	0.064	—	—	—	—	—

For all tissue in 2-compartment model and Logan plot, $n = 10$. In 3-compartment model, $n = 2$ for cerebellum and $n = 4$ for frontal lobe cortex.

0.06, and 0.01. No inverse correlation between ^{18}F-FMISO uptake and perfusion was observed.

HPLC analysis of 7 patients showed that 97%–99% of plasma radioactivity represented intact ^{18}F-FMISO 3 min after injection. Most of the ^{18}F-FMISO in plasma (92%–96%) was still intact 90 min after injection (in 1 patient after 75 min), and 1 hydrophilic metabolite, accounting for 4%–6% of plasma radioactivity, was detected. In contrast, higher ^{18}F-FMISO catabolism was found in urine, where radioactive metabolites accounted for up to 17% at 95 min after injection.

DISCUSSION

In this pilot study, we used ^{18}F-FMISO PET to investigate hypoxia in brain tumors. ^{15}O-H_2O PET was performed to compare the pattern of tumor hypoxia with perfusion. We found increased ^{18}F-FMISO uptake, indicating the presence of tumor hypoxia, in all 7 glioblastoma patients. Tissue radioactivity in glioblastoma exceeded plasma radioactivity by a factor of up to 2 within 90 min after injection. The ^{18}F-FMISO tumor distribution volumes varied between approximately 1 and 2. In contrast, the distribution volume in normal brain was always <1. The increased ^{18}F-FMISO distribution volume in tumor resulted in observable ^{18}F-FMISO retention in late PET images (150–170 min after injection). Increased ^{18}F-FMISO uptake was also found in the hemangioblastoma patient, but ^{18}F-FMISO did not accumulate in an anaplastic astrocytoma (WHO III), in a fibrillary astrocytoma (WHO II), or in a meningioma.

The presence of hypoxia appears to be a common feature of glioblastoma multiforme (*21*), and intracerebral high-grade gliomas have been found to accumulate ^{18}F-FMISO in an animal model (*22*). In humans, hypoxia in glioblastoma multiforme has also been directly measured with Eppendorf needle electrodes. Not only do the glioblastomas show severe hypoxia, but surprisingly low-grade astrocytomas and peritumoral brain tissue do so as well (*23*). Moreover, various endogenous markers of hypoxia are found to be

TABLE 3
PET Results in Tumor

Patient	Histology	^{15}O-H_2O PET perfusion in hypoxia	^{18}F-FMISO PET hypoxia	3-Compartment model					Logan plot (DV_{Logan})	^{18}F-FMISO tumor uptake 150–170 min after injection (tumor/cerebellum)
				K_1	k_2	k_3	k_4	DV_{TOT}		
1	Glioblastoma	2–3	Yes	—	—	—	—	—	—	1.87
2	Glioblastoma	2–3	Yes	0.067	0.097	0.008	0.005	1.81	0.972	1.36
3	Glioblastoma	3–4	Yes	0.067	0.116	0.030	0.029	1.17	1.068	1.21
4	Glioblastoma	1–2	Yes	—	—	—	—	—	—	1.34
5	Glioblastoma	—	Yes	0.075	0.111	0.026	0.012	2.16	1.627	2.07
6	Glioblastoma	1–2	Yes	0.045	0.089	0.030	0.019	1.31	1.097	1.31
7	Glioblastoma	4–5	Yes	0.143	0.442	0.093	0.026	1.46	1.466	1.75
8	Anaplastic astrocytoma	—	No	—	—	—	—	—	—	—
9	Fibrillary astrocytoma	—	No	—	—	—	—	—	—	—
10	Hemangioblastoma	—	Yes	0.023	0.036	0.008	0.005	1.68	0.874	1.28
11	Meningioma	—	No	0.183	0.386	0.070	0.101	0.80	0.812	0.96

Downloaded from jnm.snmjournals.org by on March 14, 2017. For personal use only.

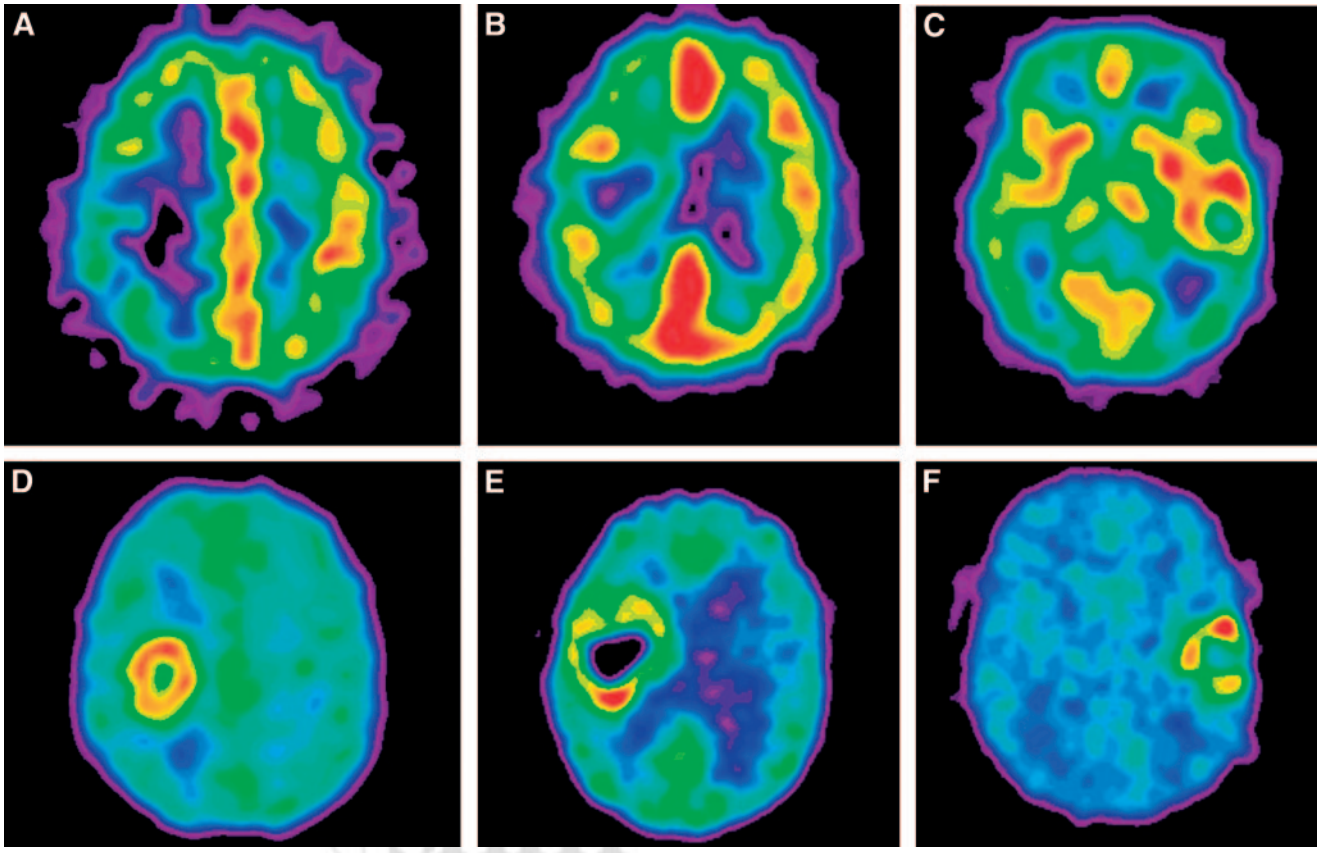


FIGURE 3. (A–C) ^{15}O-H_2O PET perfusion images in 3 patients with glioblastoma multiforme. (D–F) Corresponding late ^{18}F-FMISO PET images show tumor hypoxia in low perfusion, in intermediate perfusion with an inverse pattern compared with hypoxia, and in high perfusion. PET images are normalized to their own maximum.

overexpressed in brain tumors. For example, in glioblastoma multiforme and, to a lesser degree, in grade II and III astrocytomas, a heterogeneous pattern of the hypoxia-inducible factor 1α (HIF-1α) overexpression was found (*24*). Increased HIF-1α levels were observed in tumor areas adjacent to necrosis (e.g., in pseudopalisading cells). Consistent with that, we found increased ^{18}F-FMISO tumor uptake generally in the periphery but not in the center of a glioblastoma multiforme. The latter is expected, because only viable cells are able to accumulate ^{18}F-FMISO, and delivery to necrotic tissue is low.

To quantify the pharmacokinetics of ^{18}F-FMISO in normal brain and tumor, we used dynamic ^{18}F-FMISO PET data and the measured arterial ^{18}F-FMISO concentration for

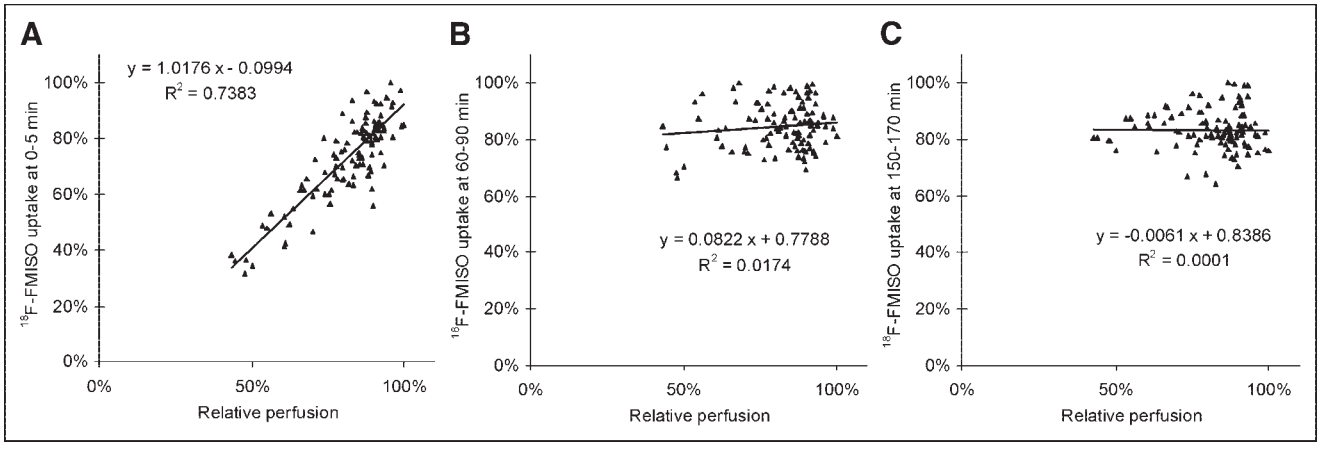


FIGURE 4. Pixel-by-pixel correlation of relative tumor perfusion with ^{18}F-FMISO accumulation in hypoxic area of glioblastoma multiforme, where ^{18}F-FMISO uptake was measured at 0–5 min (A), 60–90 min (B), and 150–170 min (C) after injection.

Downloaded from jnm.snmjournals.org by on March 14, 2017. For personal use only.

kinetic modeling with standard 2- and 3-compartment models. The calculated distribution volumes and transport rate constants (Appendix) characterize ^{18}F-FMISO as a PET agent. These parameters are especially important in the brain, because the state of the BBB can affect a radioligand's tissue delivery, confounding PET images. Our results confirm this effect for ^{18}F-FMISO. Increased K_1 values, ranging between 0.067 and 0.143 mL/min/g, were found in all glioblastomas, compared with values for K_1 of 0.010 mL/min/g in white matter and 0.023 mL/min/g in cortex, indicating a relatively slow entrance of ^{18}F-FMISO into normal brain. The increased ^{18}F-FMISO tumor uptake in glioblastoma cannot be an exclusive effect of BBB disruption resulting in increased K_1 values. Increased K_1 can account only for higher ^{18}F-FMISO uptake rates as long as tissue radioactivity does not exceed plasma radioactivity and cannot explain the continuing tracer accumulation at later scan times. In the meningioma, for example, which lacks the BBB, we found the highest value for K_1 of all brain tumors, as expected. The increased K_1 permitted delineation of the meningioma in an early ^{18}F-FMISO PET image (Fig. 1), but the tumor did not exhibit subsequent ^{18}F-FMISO accumulation and was not visualized in the late PET image. Accordingly, the ^{18}F-FMISO distribution volume in the meningioma was not increased despite a high K_1 value. Therefore, we assume that ^{18}F-FMISO accumulation in glioblastoma at late scan time does not result from an increased K_1 but from the presence of a second kinetic tissue compartment with an additional uptake rate, k_3. Thus, it is likely that late ^{18}F-FMISO PET images provide more than an image of the disrupted BBB. However, increased K_1 values in glioblastoma may confound ^{18}F-FMISO PET images at early times after injection.

We propose the total distribution volume (DV_{TOT}) of a 3-compartment model for absolute quantification of ^{18}F-FMISO tumor uptake, where values >1 indicate tumor uptake due to $k_3 > 0$ and, therefore, suggest the presence of hypoxia. Alternatively, the ^{18}F-FMISO distribution volume can be determined graphically using a Logan plot, avoiding assumptions about the number of underlying tissue compartments. Finally, because the distribution of ^{18}F-FMISO in the brain is very uniform, simple radioactivity ratios using ROI analysis can be used for relative quantification of static ^{18}F-FMISO at late times after injection. Ratios of tumor and cerebellum radioactivity likely contain the same information as DV_{TOT} for the detection of tumor hypoxia (Table 3).

We assume that no other active mechanism than the binding of bioreductive metabolites, dependent on the presence of hypoxia, leads to increased ^{18}F-FMISO tumor uptake. Additional factors (e.g., tumor viability, the presence of necrosis, or cellular density) may modulate the degree of ^{18}F-FMISO tumor uptake. Moreover, cellular ^{18}F-FMISO uptake and retention depend nonlinearly on the pO_2 (*25*). Therefore, although DV_{TOT} or DV_{Logan} allow quantitative estimates of ^{18}F-FMISO uptake, they cannot be directly related to tumor pO_2.

An often debated issue in the use of ^{18}F-FMISO concerns stability in vivo, because this is a prerequisite for specific tumor uptake in hypoxic areas. Although a relatively high metabolism of ^{18}F-FMISO in plasma and urine in mice hinders tumor imaging (*26*), we find most of the plasma radioactivity to be intact ^{18}F-FMISO until 90 min after injection in humans and >80% of ^{18}F-FMISO to appear as intact parent substance in the urine. We conclude that nonspecific radioactivity uptake in human tumors as a result of ^{18}F-FMISO plasma metabolites is not relevant, and no correction for metabolites is needed if ^{18}F-FMISO plasma concentration is measured to provide an arterial input curve. In this respect, the use of ^{18}F-FMISO represents no disadvantage compared with other nitroimidazole derivatives.

An important aspect of this study was investigating the influence of perfusion on ^{18}F-FMISO uptake in brain tumors (i.e., we wanted to exclude the possibility that ^{18}F-FMISO PET images simply reflect tumor perfusion). Pixel-per-pixel comparisons of ^{18}F-FMISO with ^{15}O-H_2O PET images yielded a positive correlation of early ^{18}F-FMISO uptake with perfusion (Fig. 4A), as for almost any radioligand used in nuclear medicine. This correlation was only minimal or already lost at 60–90 min after injection (Fig. 4B), and ^{18}F-FMISO images at 150–170 min after injection were independent of perfusion with a single exception (Fig. 4C). These results are a precondition if ^{18}F-FMISO retention at late time in brain tumors is to provide information other than perfusion. Static PET images should therefore not be obtained earlier than 2–2.5 h after injection.

We found different patterns of hypoxia and perfusion in patients with glioblastomas (Fig. 3), showing apparently that hypoxia occurs independently of perfusion. All glioblastomas investigated showed hypoxia. Only 2, however, revealed hypoperfusion, whereas hypoxia occurred in tumor areas with intermediate or high perfusion in the other 4 tumors. As illustrated in Figure 3, these patterns were observed in the tumor periphery, where tissue is considered most active with regard to proliferation and infiltration of surrounding brain tissue. This hypoxia–hyperperfusion pattern is unexpected, because in general one would expect hypoxia to occur in low perfusion. The latter has been demonstrated in the myocardium of dogs, where Martin et al. (*27*) demonstrated an inverse correlation between perfusion and ^{18}F-FMISO uptake after complete or partial occlusion of the left anterior descending coronary artery. Animal studies using human glioma xenografts also demonstrated an inverse relationship between the density of perfused vessels and the fraction of hypoxic tumor cells (*7*). That study showed that the intensity of hypoxia staining corresponds to increasing distances of tumor cells from vessels, making an inverse correlation between perfusion and hypoxia conceivable. Groshar et al. (*28*) used ^{99m}Tc-hexamethylpropyleneamine oxime and ^{123}I-iodoazomycin arabinoside SPECT in patients to demonstrate an inverse relation be-

Downloaded from jnm.snmjournals.org by on March 14, 2017. For personal use only.

tween perfusion and hypoxia in nonglial tumors. However, all 4 glioblastoma patients in that study showed decreased perfusion and absence of hypoxia.

A mismatch between hypoxia and perfusion may be characteristic of malignant brain tumors, which exhibit a discrepancy between high vascularization and a comparably low, possibly inefficient perfusion (*29*). Differentiation between diffusion-limited (chronic) and perfusion-limited hypoxia has been proposed (*3*). Whether these 2 types are reflected in the patterns observed in our present study and that of Groshar (*28*) cannot be answered, because the findings of Rijken et al. (*7*) and Tochon-Danguy et al. (*22*) were obtained in animals. It is not known whether patterns of hypoxia and perfusion change with the evolution of glioblastoma. Their impact on prognosis and response to therapy remains a subject for future study.

CONCLUSION

We performed ^{18}F-FMISO and ^{15}O-H_2O PET in brain tumors to measure tumor hypoxia and perfusion. Increased ^{18}F-FMISO tumor retention at late scan time was found predominantly in glioblastoma multiforme, and this was associated with an increased ^{18}F-FMISO tumor distribution volume. This finding could not be explained by nonspecific perfusion effects or by BBB disruption alone. We used the ^{18}F-FMISO distribution volume as a quantitative criterion for hypoxia, where values >1 indicated active binding and suggested the presence of tumor hypoxia. ^{18}F-FMISO accumulated in both hypo- and hyperperfused tumor regions, suggesting that hypoxia in glioblastoma may develop irrespective of the magnitude of perfusion. Simple tumor-to-cerebellum ratios at late scan time provide a good estimate of the ^{18}F-FMISO distribution volume in the clinical setting.

APPENDIX

Description of Compartment Models

Kinetic modeling was performed with dynamic ^{18}F-FMISO PET data during the first scan from 0–90 min after injection using the commercially available software PMOD (*19*). The tissue time–activity curves measured by PET and the arterial plasma concentration were used to quantify transport rates and distribution volume of ^{18}F-FMISO with standard 2- and 3-compartment models. The 3-compartment model consisted of 1 intravascular and 2 tissue compartments, where the transport rate constants K_1 and k_2 describe the ^{18}F-FMISO uptake and washout rates from plasma to the first tissue compartment, respectively, and the transport rate constants k_3 and k_4 represent the ^{18}F-FMISO exchange between the first and the second tissue compartment. The intravascular compartment was set to a fixed volume of 0.05 (i.e., spillover by blood radioactivity was assumed to account for 5% of tissue radioactivity). Curve fitting determined the transport rates K_1, k_2, k_3, and k_4. Briefly, a model tissue curve was calculated using the arterial plasma radioactivity curve and the model transport rates K_1–k_4, and the fitting algorithm tried to minimize the difference between the measured tissue radioactivity and the model curve. We used an iterative fitting algorithm with Marquardt–Levenberg optimization, a standard option in the software PMOD (*19,30*). The total ^{18}F-FMISO distribution in both tissue compartments was calculated as $DV_{TOT} = K_1/k_2 \times (1 + k_3/k_4)$. Alternatively, we used a 2-compartment model consisting of an intravascular compartment with a constant volume of 0.05 and a single tissue compartment. Parameters of the 2-compartment model were K_1' and k_2', and the ^{18}F-FMISO distribution volume was calculated as $DV' = K_1'/k_2'$. This model has only 2 free parameters, K_1' and k_2', and, therefore, promises fits of higher robustness.

Model Evaluation and Results

The goodness of fit was evaluated using the Akaike criterion (AIC) as described by Hawkins et al. (*31*). Generally, low AIC values indicate the appropriateness of the model to explain PET data with a minimum of free parameters. Introduction of an excess parameter does not impair the model fit but leads to an increased AIC value. This indicates that the parameter is not necessary to explain PET data and, therefore, not reliable. On the other hand, too few free parameters may prevent the model curve from being fitted well to PET data, resulting in increased AIC values.

To determine the optimal model to explain the ^{18}F-FMISO kinetics in brain tissue, we successively increased the degrees of freedom of the 3-compartment model by stepwise introduction of K_1, k_2, k_3, and k_4, until the minimum AIC value was reached. For example, if fitting with a free k_3 resulted in a lower AIC value than a fit with k_3 kept at zero, this was interpreted as evidence for the presence of a k_3 and, therefore, of a second kinetic tissue compartment. Consequently, we used the 3-compartment model only if the AIC criterion indicated the presence of 2 kinetic tissue compartments. This was true in all tumors and also in normal brain in some instances. In all other cases, the 2-compartment model was used instead, particularly in normal brain. In addition, we used the AIC to determine reversibility or irreversibility of ^{18}F-FMISO tissue uptake. Thus, we checked whether the AIC increased if k_2 or k_4 was held constant at zero in the 2- or 3-compartment model, suggesting reversibility of binding, because k_2 and k_4 are >0.

In normal brain, ^{18}F-FMISO generally distributed passively in a single reversible tissue compartment with $DV' < 1$ (Table 2). Reversibility of ^{18}F-FMISO uptake could always be established (i.e., keeping k_2 at zero resulted in significantly worse fits with higher values for the AIC). However, kinetic analysis showed the presence of 2 tissue compartments in the frontal cortex in 4 patients and in the cerebellum in 2 patients. We have no explanation for the sporadic presence of 2 ^{18}F-FMISO tissue compartments in normal brain. In no cases did analysis of the AIC indicate

Downloaded from jnm.snmjournals.org by on March 14, 2017. For personal use only.

the presence of a second tissue compartment in white matter. There was good agreement between DV_{TOT} and DV′ (Table 2). Thus, the choice of the model did not play an important role in the resulting value of the ^{18}F-FMISO distribution volume in normal brain. Determination of the ^{18}F-FMISO distribution volume by a Logan plot yielded values that were comparable with the 2- and 3-compartment models in the frontal cortex and cerebellum, but values in white matter were somewhat lower. In tumor, increased ^{18}F-FMISO uptake at late scan times was associated with $DV_{TOT} > 1$ (Table 3). In these instances, analysis of the AIC indicated the presence of 2 kinetic tissue compartments (i.e., the goodness of fit always improved with the 3-compartment model).

^{18}F-FMISO tumor binding was found to be reversible in 4 patients, where holding k_4 to zero resulted in worse data fits with increased AIC values. In 3 patients, $k_4 > 0$ could also be determined, but the goodness of fit was not impaired if k_4 was kept at zero. Therefore, reversibility of the second tissue compartment could not be proven in these patients. On one hand, reversibility of ^{18}F-FMISO tumor binding is surprising, because the covalent binding of bioreductive ^{18}F-FMISO metabolites in hypoxic cells is expected to be irreversible (*32*). On the other hand, isolated cell studies have indicated that some metabolites of radiolabeled misonidazole may "back diffuse" from the cells at a low rate, which can possibly explain our finding (*33*).

ACKNOWLEDGMENTS

We thank Professor Gustav K. von Schulthess and Professor Alfred Buck for placing the PET infrastructure of the University Hospital Zurich at our disposal and for technical support. Also, we thank Thomas Berthold and Claudia Keller for assistance in PET and Erika Sinnig for laboratory work. We also thank Dr. John Missimer for assistance in editing the manuscript.

REFERENCES

1. Nias AHW. *An Introduction to Radiobiology.* 2nd ed. London, UK: Wiley & Sons; 1998.
2. Gray LH, Conger AD, Ebert M, et al. The concentration of oxygen dissolved in tissues at the time of irradiation as a factor in radiotherapy. *Br J Radiol.* 1953;26:638–648.
3. Airley RE, Monaghan JE, Stratford IJ. Hypoxia and disease: opportunities for novel diagnostic and therapeutic prodrug strategies. *Pharm J.* 2000;264:666–673.
4. Ikeda E, Achen MG, Breier G, et al. Hypoxia-induced transcriptional activation and increased mRNA stability of vascular endothelial growth factor in C6 glioma cells. *J Biol Chem.* 1995;270:19761–19766.
5. Kleihues P, Cavanee WK. Tumours of the nervous system. *Pathology and Genetics: World Health Organization Classification of Tumors.* Lyon, France: IARC Press; 2000.
6. Bernsen HJ, Rijken PF, Peters H, et al. Hypoxia in a human intracerebral glioma model. *J Neurosurg.* 2000;93:449–454.
7. Rijken PF, Bernsen HJ, Peters JP, et al. Spatial relationship between hypoxia and the (perfused) vascular network in a human glioma xenograft: a quantitative multi-parameter analysis. *Int J Radiat Oncol Biol Phys.* 2000;48:571–582.
8. Chapman JD, Engelhardt EL, Stobbe CC, et al. Measuring hypoxia and predicting tumor radioresistance with nuclear medicine assays. *Radiother Oncol.* 1998;46:229–237.
9. Rasey JS, Koh WJ, Grierson JR, et al. Radiolabeled fluoromisonidazole as an imaging agent for tumor hypoxia. *Int J Radiat Oncol Biol Phys.* 1989;17:985–991.
10. Lewis J, Laforest R, Buettner T, et al. Copper-64-diacetyl-bis(N4-methylthiosemicarbazone): an agent for radiotherapy. *Proc Natl Acad Sci USA.* 2001;98:1206–1211.
11. Gronroos T, Eskola O, Lehtio K, et al. Pharmacokinetics of ^{18}F-FETNIM: a potential marker for PET. *J Nucl Med.* 2001;42:1397–1404.
12. Dolbier WR Jr, Li AR, Koch CJ, et al. [^{18}F]-EF5, a marker for PET detection of hypoxia: synthesis of precursor and a new fluorination procedure. *Appl Radiat Isot.* 2001;54:73–80.
13. Lehtio K, Oikonen V, Nyman S, et al. Quantifying tumour hypoxia with fluorine-18 fluoroerythronitroimidazole ([^{18}F]FETNIM) and PET using the tumour-to-plasma ratio. *Eur J Nucl Med Mol Imaging.* 2003;30:101–108.
14. Rasey JS, Koh WJ, Evans ML, et al. Quantifying regional hypoxia in human tumors with positron emission tomography of [^{18}F]fluoromisonidazole: a pretherapy study of 37 patients. *Int J Radiat Oncol Biol Phys.* 1996;36:417–428.
15. Whitmore GF, Varghese AJ. The biological properties of reduced nitroheterocyclics and possible underlying biochemical mechanisms. *Biochem Pharmacol.* 1986;35:97–103.
16. Valk PE, Mathis CA, Prados MD, et al. Hypoxia in human gliomas: demonstration by PET with fluorine-18-fluoromisonidazole. *J Nucl Med.* 1992;33:2133–2137.
17. Leenders KL. PET: blood flow and oxygen consumption in brain tumors. *J Neurooncol.* 1994;22:269–273.
18. Lim JL, Berridge MS. An efficient radiosynthesis of [^{18}F]fluoromisonidazole. *Appl Radiat Isot.* 1993;44:1085–1091.
19. Mikolajczyk K, Szabatin M, Rudnicki P, et al. A JAVA environment for medical image data analysis: initial application for brain PET quantitation. *Med Inform (Lond).* 1998;23:207–214.
20. Logan J, Fowler JS, Volkow ND, et al. Graphical analysis of reversible radioligand binding from time–activity measurements applied to [N-^{11}C-methyl]-(-)-cocaine PET studies in human subjects. *J Cereb Blood Flow Metab.* 1990;10:740–747.
21. Brat DJ, Castellano-Sanchez AA, Hunter SB, et al. Pseudopalisades in glioblastoma are hypoxic, express extracellular matrix proteases, and are formed by an actively migrating cell population. *Cancer Res.* 2004;64:920–927.
22. Tochon-Danguy HJ, Sachinidis JI, Chan F, et al. Imaging and quantitation of the hypoxic cell fraction of viable tumor in an animal model of intracerebral high-grade glioma using [^{18}F]fluoromisonidazole (FMISO). *Nucl Med Biol.* 2002;29:191–197.
23. Collingridge DR, Piepmeier JM, Rockwell S, et al. Polarographic measurements of oxygen tension in human glioma and surrounding peritumoural brain tissue. *Radiother Oncol.* 1999;53:127–131.
24. Zagzag D, Zhong H, Scalzitti JM, et al. Expression of hypoxia-inducible factor 1-alpha in brain tumors: association with angiogenesis, invasion, and progression. *Cancer.* 2000;88:2606–2618.
25. Gross MW, Karbach U, Groebe K, et al. Calibration of misonidazole labeling by simultaneous measurement of oxygen tension and labeling density in multicellular spheroids. *Int J Cancer.* 1995;61:567–573.
26. Rasey JS, Hofstrand PD, Chin LK, et al. Characterization of [^{18}F]fluoroetanidazole, a new radiopharmaceutical for detecting tumor hypoxia. *J Nucl Med.* 1999;40:1072–1079.
27. Martin GV, Caldwell JH, Graham MM, et al. Noninvasive detection of hypoxic myocardium using fluorine-18-fluoromisonidazole and positron emission tomography. *J Nucl Med.* 1992;33:2202–2208.
28. Groshar D, McEwan AJ, Parliament MB, et al. Imaging tumor hypoxia and tumor perfusion. *J Nucl Med.* 1993;34:885–888.
29. Vajkoczy P, Menger MD. Vascular microenvironment in gliomas. *J Neurooncol.* 2000;50:99–108.
30. Marquardt DW. An algorithm for least squares estimation of nonlinear parameters. *J Soc Industr Appl Math.* 1963;11:431–441.
31. Hawkins RA, Phelps ME, Huang SC. Effects of temporal sampling, glucose metabolic rates, and disruptions of the blood–brain barrier on the FDG model with and without a vascular compartment: studies in human brain tumors with PET. *J Cereb Blood Flow Metab.* 1986;6:170–183.
32. Casciari JJ, Graham MM, Rasey JS. A modeling approach for quantifying tumor hypoxia with [F-18]fluoromisonidazole PET time–activity data. *Med Phys.* 1995;22:1127–1139.
33. Rasey JS, Grunbaum Z, Magee S, et al. Characterization of radiolabeled fluoromisonidazole as a probe for hypoxic cells. *Radiat Res.* 1987;111:292–304.

Downloaded from jnm.snmjournals.org by on March 14, 2017. For personal use only.

JNM The Journal of NUCLEAR MEDICINE

Assessment of Hypoxia and Perfusion in Human Brain Tumors Using PET with ^{18}F-Fluoromisonidazole and ^{15}O-H_2O

Matthias Bruehlmeier, Ulrich Roelcke, Pius A. Schubiger and Simon Mensah Ametamey

J Nucl Med. 2004;45:1851-1859.

This article and updated information are available at:
http://jnm.snmjournals.org/content/45/11/1851

Information about reproducing figures, tables, or other portions of this article can be found online at:
http://jnm.snmjournals.org/site/misc/permission.xhtml

Information about subscriptions to JNM can be found at:
http://jnm.snmjournals.org/site/subscriptions/online.xhtml

The Journal of Nuclear Medicine is published monthly.
SNMMI | Society of Nuclear Medicine and Molecular Imaging
1850 Samuel Morse Drive, Reston, VA 20190.
(Print ISSN: 0161-5505, Online ISSN: 2159-662X)

© Copyright 2004 SNMMI; all rights reserved.

SNMMI SOCIETY OF NUCLEAR MEDICINE AND MOLECULAR IMAGING